IEEE Access
Multidisciplinary ⋮ Rapid Review ⋮ Open Access Journal

Received August 6, 2021, accepted August 22, 2021, date of publication August 25, 2021, date of current version September 2, 2021.

Digital Object Identifier 10.1109/ACCESS.2021.3107802

Compensation Method for Shadow Effect of Mine Ultrasonic Anemometer

ZHENGUAN CAO, ZONGTANG ZHANG, RUI LI, XUN YANG, AND ZHENGHANG ZHOU
School of Electrical and Information Engineering, Anhui University of Science and Technology, Huainan 232001, China

Corresponding author: Zongtang Zhang (ztzhang0326@163.com)

This work was supported in part by the National Key Research and Development Program of China under Grant 2018YFC0808100.

ABSTRACT The ultrasonic anemometer is widely used in the field of wind speed measurement in the coal mine. To compensate for the error of wind speed caused by the shadow effect, we propose a method based on kernel extreme learning machine combined with particle swarm optimization (PSO-KELM). Firstly, we established and analyzed the simulation experiment by computational fluid dynamics (CFD). Secondly, we used the PSO to optimize the parameters of the KELM. The evaluation indexes of the PSO-KELM on the test set are better than other regression models. Finally, the accuracy of the PSO-KELM was verified by experimental data obtained by the ultrasonic anemometer in the wind tunnel. The results show that the compensation effect of the PSO-KELM is better than other regression models. The PSO-KELM model proposed in the paper can effectively compensate for the error of wind speed, and make the measurement results of the ultrasonic anemometer more accurate.

INDEX TERMS Ultrasonic anemometer, coal mine, shadow effect, kernel extreme learning machine, error compensation.

I. INTRODUCTION

Accurate measurement of wind speed in coal mine roadway is one of the necessary guarantees for safety production [1], [2]. By accurately measuring the wind speed of the coal mine roadway, we can calculate and analyze the migration process of gas, dust, and other harmful gases [3]. And we can control the distribution of temperature and humidity in the coal mine roadway in real-time. Traditional anemometers are used widely, but they have the limitation of low sensitivity, and they need human intervention [4], [5]. In the complex environment of high humidity and high dust in the coal mine, the accuracy of traditional anemometers is low. Therefore, to realize the effective monitoring of ventilation parameters, people need an intelligent mine wind anemometer with strong stability and high measurement accuracy urgently.

With the development of science and technology, the technology of ultrasonic wind measurement is gradually mature. The ultrasonic anemometer has many advantages, such as no rotating parts, easy installation, stable performance, low maintenance cost, and no start-up wind speed [6]–[8]. However, in the measurement process of the ultrasonic anemometer, the specific wake area will be formed behind transducers on the windward side, which will make the wind speed on the leeward side lower. This phenomenon is called the shadow effect. Due to the shadow effect, there is a deviation in the measurement process of wind speed. Researchers have studied the influence of the shadow effect on the ultrasonic anemometer. Horst *et al.* [9] studied the dependence of transducer shadowing on sonic path geometry, wind direction, and atmospheric stability with simulations, and proposed that the flow distortion within a non-orthogonal CSAT3 sonic anemometer is primarily due to transducer shadowing. Nevertheless, there is a principal shortcoming in this method, that is, the results depend on the comparison between sonics and the correction of dimensionless turbulence statistics, as well as the limited wind-direction range. With this in mind, Nasab *et al.* [10] proposed the compensation function to calibrate the sensor outputs by several wind-tunnel tests on the single-axis ultrasonic anemometer. They placed the signal path of the ultrasonic anemometer at various azimuthal angles concerning the wind direction. This method works well when the anemometer rotates continuously around its vertical axis. While in the actual measurement process, it is difficult to compensate for the error caused by the shadow effect quickly. And the process of obtaining data is complex. Given this, Yang and Chen [11] proved the numerical method can effectively verify the influence of transducer shadowing on the

The associate editor coordinating the review of this manuscript and approving it for publication was Wei Xiang.

wind velocity by the data obtained from Fluent software. The compensation method they proposed is effective to analyze the influence of the shadow effect on measurement results through simulations. And the wind speed error is reduced to 1.74 % by this method. However, we have higher accuracy requirements in some cases, so the measurement accuracy of this method still needs to be further improved. They might consider using advanced learning methods to process data. The shadow effect has a great influence on the accurate measurement of wind speed. Therefore, it is very important for us to solve the measurement error caused by the shadow effect. Unfortunately, there is still a lack of specific methods to compensate for the wind speed of the ultrasonic anemometer and make the measurement results more accurate.

With the significant improvement of computer performance, the machine learning algorithm has been used in many fields widely [12]–[15]. The regression algorithm is a typical classification in the machine learning algorithm. There are many common regression algorithms, such as support vector regression (SVR) [16], [17], extreme learning machine (ELM) [18], [19], back-propagation neural networks (BPNN) [20], [21], and decision tree (DT) [22]–[24], etc. The kernel extreme learning machine uses the method of stable kernel mapping to replace the random generation of some parameters in ELM, and it has the advantages of fewer adjustment parameters and fast convergence [25]–[27]. KELM has superior performance in practical application. Lu *et al.* [28] realized the single-step prediction of burning zone temperature by combining the sliding time window and KELM method. As we can see, the single average running time of KELM is 0.0002s, which is significantly shorter than SVR. The KELM method greatly reduced the single average running time of model training and prediction. Shamshirband *et al.* [29] proposed that the potential of KELM to predict the daily horizontal global solar radiation from the maximum and minimum air temperatures is appraised. They compared the KELM regression model with the SVR model, and the evaluation index of the KELM model is better than SVR. The results show that KELM regression has a good prediction effect. In addition to comparing with SVR, we can also compare with other regression models. With this in mind, Fu *et al.* [30] proposed a KELM technique to predict the indicators of Holstein dry cows' diet digestible energy (DE) and energy digestibility (ED) and compared the prediction effect of the KELM model with other regression models. The prediction results showed that the KELM was superior to other methods in most performance indexes. These studies show that the KELM model has good performance in the field of prediction. In addition, KELM has been successfully applied to short-term passenger flow prediction [31], short-term wind speed forecasting [32], smart grid protection [33], etc. Based on the good regression performance of KELM, it is selected to compensate for the shadow effect of the ultrasonic anemometer. Although the KELM regression model has excellent performance, it is sensitive to the parameter setting. It takes a lot of time to determine the optimal parameters of KELM manually. Therefore, we need to adopt the common algorithm to optimize the parameters of the KELM model.

Particle swarm optimization (PSO) is derived from the study of the predation behavior of birds. The basic idea of the particle swarm optimization algorithm is to find the optimal solution through cooperation and information sharing among individuals in the group. It is easy to implement, and it does not need to adjust many parameters [34], [35]. Zhu *et al.* [36] used PSO to optimize the parameters of chaos recurrent adaptive neuro-fuzzy information system (CRANFIS) and predicted the ground vibration. As we can see, the PSO model can effectively improve the limitations of the CRANFIS algorithm, such as slow convergence, etc. The model is more reliable and accurate after optimization. And the effect is better than ANN and other models. In addition, Tang *et al.* [37] used PSO to optimize the parameters of SVR and predicted the cooling capacity and system coefficient of performance of the battery thermal management system. They compared the PSO-SVR model with the SVR model. The results show that the effect of the PSO-SVR model was better than the SVR model. By considering these application examples, the PSO algorithm is selected as the optimization algorithm of the KELM model.

Based on these, we propose an error compensation method for the wind speed of the mine ultrasonic anemometer based on Fluent and the PSO-KELM model. First of all, we built the hardware model and designed a mine high-precision ultrasonic anemometer based on the ultrasonic time-difference method. However, if we study the influence of the shadow effect systematically, we need immense experimental data. The operation process of obtaining these data in the wind tunnel is very complex, and the cost of the experiment is high. Therefore, we consider using the theoretical analysis method to study the error compensation method for wind speed. Computational fluid dynamics (CFD) is widely used in aviation, meteorology, industry, and chemistry [38]–[43]. In the paper, the shadow effect of ultrasonic anemometer under different wind speeds is modeled and simulated by Fluent software. We analyze the influence of the shadow effect on the ultrasonic anemometer. We use simulation data to provide sample data for the error compensation algorithm and establish the KELM regression model. We use the PSO algorithm to optimize the parameters of KELM and use the PSO-KELM regression model to compensate for the wind speed of the ultrasonic anemometer. The accuracy of the PSO-KELM regression model is verified by the measured data obtained from the wind tunnel. The methods and results of the paper provide a certain reference value for the error correction of the wind speed. At the same time, it realizes the intelligent detection of wind speed in the coal mine roadway and ensures the efficiency of tasks in the coal mine.

This research aimed to explore whether PSO-KELM is suitable for the error compensation of wind speed. Section 1 contains the literature review. The rest of the paper is organized as follows: Section 2 contains principles and

methods. The construction and optimization of the KELM model are described in this part. Section 3 contains modeling and simulation. Section 4 contains the results and discussion. The KELM model is compared with the SVR, BP, ELM, and DT model, respectively. And the KELM model is optimized by the PSO algorithm. At the same time, the performance of the model is compared according to the evaluation index. Section 5 contains the conclusions of this study.

II. PRINCIPLES AND METHODS

A. PRINCIPLE OF ULTRASONIC TIME-DIFFERENCE WIND MEASUREMENT

When the measurement of wind speed parameters in the coal mine is inaccurate, the number of accidents will increase. As we can see in Table 1, these accidents that occurred in the coal mines have caused a large number of casualties and economic losses. Therefore, it is necessary for us to improve the measurement accuracy of wind speed.

TABLE 1. Accidents occurred in the coal mines.

Time	Location	Cause of the accident	Consequences
2003.12.17	Beijing	The ventilation system is unreasonable, and the detection of ventilation parameters is unreliable.	Four workers died of suffocation and poisoning.
2006.04.29	Shanxi	The air volume is seriously insufficient, and the facilities are not perfect.	Thirty-two workers died and seven were injured, with a direct economic loss of 10.31 million yuan.
2012.08.29	Sichuan	Incomplete safety monitoring facilities and unreliable ventilation parameters.	Forty-eight workers died and fifty-four were injured, with a direct economic loss of 49.8 million yuan.
2016.10.31	Chongqing	The ventilation parameter detection system is unreliable.	Thirty-three workers died and one was injured, with a direct economic loss of 36.82 million yuan.

Normally, we calculate the wind speed by the ultrasonic time-difference method. Figure 1 shows the schematic diagram of the principle of the ultrasonic time-difference method. We can see two pairs of transmitter-receiver ultrasonic transducer probes on the ultrasonic anemometer. Their positions are constant. They emit ultrasonic pulse trains at a fixed frequency. In the presence of wind, the wind speed will have the effect of superposition or reduction on the propagation velocity of ultrasonic, and it will cause two kinds of conditions: tailwind or headwind. We calculate the wind speed by measuring the propagation time of ultrasonic waves between probes. In Figure 1, the east-west direction corresponds to the x-axis, and the north-south direction corresponds to the y-axis. In the presence of wind, the wind speed (v) can vectorially decompose into the wind speed component (v_y) in the y-axis and the wind speed component (v_x) in the x-axis.

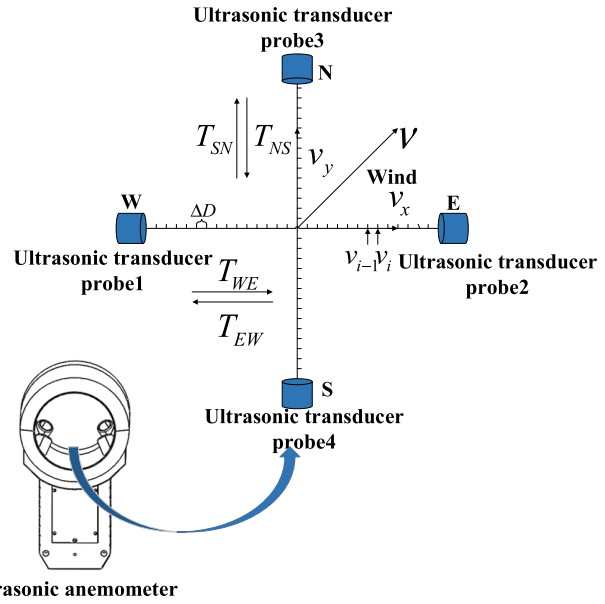

FIGURE 1. Schematic diagram of the principle of the ultrasonic time-difference method.

The distance between each pair of opposite-type ultrasonic probes is D.

In the y-axis direction, the T_{SN} is the propagation time in the tailwind, and T_{NS} is the propagation time in the headwind. At the same time, in the x-axis direction, the T_{WE} is the propagation time in the tailwind, and T_{EW} is the propagation time in the headwind. In the y-axis direction, the wind speed (v_y) can be expressed as follow:

$$v_y = D\,(T_{NS} - T_{SN})\big/(2T_{SN}T_{NS}) \tag{1}$$

Similarly, the wind speed (v_x) can be expressed as follow:

$$v_x = D\,(T_{EW} - T_{WE})\big/(2T_{WE}T_{EW}) \tag{2}$$

When T_{SN}, T_{NS}, T_{WE}, and T_{EW} are measured, the wind speed (v) can be expressed as follow:

$$v = D\sqrt{(1/T_{SN} - 1/T_{NS})^2 + (1/T_{WE} - 1/T_{EW})^2} \tag{3}$$

Obviously, the core of the ultrasonic time-difference method is to measure the propagation time. As we can know, the actual process of the wind tunnel test is very complex and the test cost is high. With this in mind, we should study the influence of shadow effect on wind speed by simulation method. In the actual processing process, we just need to record the propagation time of ultrasonic waves, and we can quickly calculate the wind speed at this time. However, in the simulation process of Fluent, it is difficult to get the propagation time. The simulation data obtained by Fluent are just the wind speed at each point of the wind tunnel in the simulation model. Therefore, we should apply the ultrasonic time-difference method to the simulation process of Fluent. The flow chart of the practical application of the ultrasonic time-difference method is shown in Figure 2. Due to the influence of the shadow effect, the propagation velocity of each point on

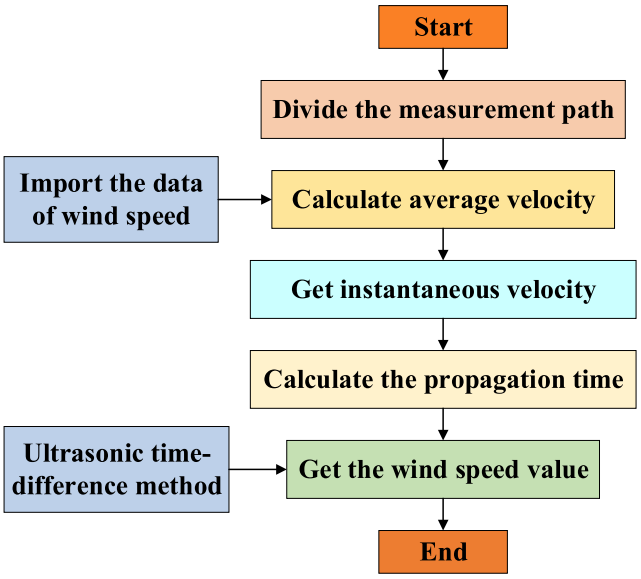

FIGURE 2. Flow chart of the ultrasonic time-difference method.

the measurement path will change unevenly, and wind speed change along the measurement path. Therefore, we adopt the infinitesimal method and divide the measurement path into N segments averagely. Each segmentation point is taken as a detection point.

In Figure 1, the length of each segment (ΔD) is D/N, then the average velocity of each segment is $(v_{N-1} + v_N)/2$. When N tends to infinity, the length of each segment tends to zero. At this time, the average velocity of each segment can be used to replace the instantaneous velocity. The velocity of each point on the measurement path can be obtained by Fluent software, and then the propagation time of each segment can be obtained. After superposition, we can obtain the propagation time between probes. The specific formulas of the propagation time are as follows:

$$t^+ = \sum_{i=1}^{N} \Delta t_i^+ = \sum_{i=1}^{N} \frac{\Delta D}{v_C + (v_i + v_{i-1})/2} \tag{4}$$

$$t^- = \sum_{i=1}^{N} \Delta t_i^- = \sum_{i=1}^{N} \frac{\Delta D}{v_C - (v_i + v_{i-1})/2} \tag{5}$$

where t^+ is the propagation time in the tailwind and t^- is the propagation time in the headwind. Δt_i is the propagation time in each segment, v_C is the propagation speed of the ultrasonic wave, and v_i is the wind speed of the i-th detection point.

According to formulas (4) and (5), if we want to get accurate wind speed, the key is to get the wind speed at $N + 1$ detection points. But each detection point is affected by the shadow effect differently. Therefore, we simulate the influence of the shadow effect on the ultrasonic anemometer in the wind tunnel accurately by CFD. After obtaining sample data of each detection point, we use the regression model of the machine learning algorithm to compensate for the error of sample data and obtain a more accurate wind speed value.

B. PRINCIPLE OF REGRESSION ALGORITHM

1) KELM

ELM is a novel single-hidden layer feedforward neural network (SLFN). The input weight and hidden layer offset of ELM can be assigned randomly. There is no need to update through multiple iterations.

KELM replaces the feature mapping in ELM with kernel matrix, which makes KELM more stable and accurate than ELM.

The schematic diagram of ELM is shown in Figure 3.

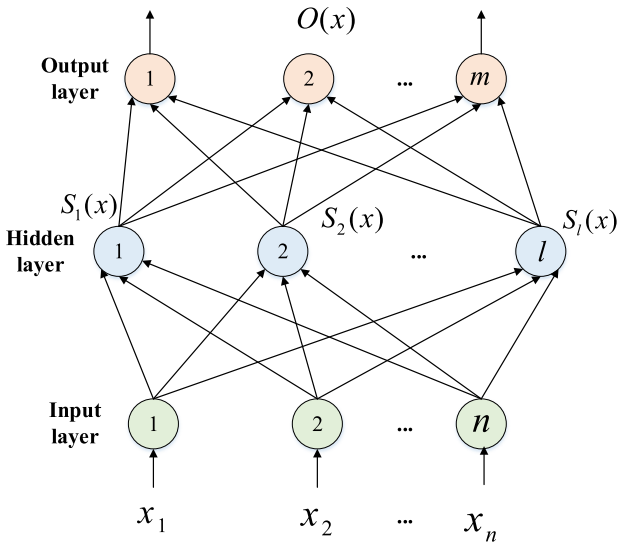

FIGURE 3. Schematic diagram of ELM.

As we can see in Figure 3, suppose n samples constitute sample sets: $A = \{(x_1, y_1), (x_2, y_2), \cdots (x_n, y_n)\}$. $y_1 = (y_1, y_2, \ldots, y_n)$, l is the number of nodes in the hidden layer. $s(x)$ is the output of the hidden layer. $O(x)$ is the output function of ELM. The formula of $O(x)$ is as follow:

$$O_l(x) = \sum_{i=1}^{l} \beta_i s_i(x) = s(x)\beta \tag{6}$$

where β_i is the weight between the i-th hidden layer neuron and the output layer, $s_i(x)$ is the output vector generated by the i-th hidden layer node. $\hat{\beta} = s^{\dagger}T$ can be used to calculate the optimal output weight ($\hat{\beta}$) of β, where $s^{\dagger}$ is the Moore-Penrose generalized inverse of s. In the paper, the kernel function is used to replace the random initial number in ELM, so the output function of KELM is as follow:

$$O(x) = \begin{bmatrix} K(x, x_1) \\ \vdots \\ K(x, x_N) \end{bmatrix}^T (\frac{I}{C} + ss^T)^{-1} Y \tag{7}$$

where C is the regularization coefficient and $K(x, x_N)$ is the kernel matrix. The kernel functions in KELM include linear kernel function, polynomial kernel function and Gaussian (RBF) kernel function. The function of RBF is

as follow:

$$k(x, y) = \exp(-\|x - y\|^2 / k_1) \tag{8}$$

where k_1 is the parameter of the kernel function.

2) PARAMETER OPTIMIZATION OF THE KELM

Particle swarm optimization (PSO) is a parallel optimization algorithm that imitates the birds' predation behavior. It has the characteristics of fast convergence and strong global searchability. Each particle in the particle swarm represents the possible solution of a problem, and the intelligence of solving the problem is realized through the information interaction between individual particles.

In the training process of the KELM, the type of kernel function, the parameters of the kernel function, and the penalty coefficient play an important role in the learning accuracy and generalization ability of the KELM model. Therefore, we use the PSO algorithm to optimize the parameters of the KELM.

The processing flow of the PSO-KELM regression model is shown in Figure 4. As we can see, we need to optimize the parameters of the KELM model and obtain the error compensation method in the next step.

The Gaussian kernel function is used as the kernel function. The penalty coefficient (C) is the tolerance of error, and g is the parameter of the RBF function. We get a good regression model by finding the best parameters C and g. The basic processes of KELM parameter optimization by PSO are as follows:

(1) Divide the training set and the test set of the KELM model, and select the search interval of C and g;

(2) Initialization particle swarm optimization randomly, and determine the position and speed;

(3) The calculation and evaluation of particle fitness values are carried out;

(4) Change individual speed and position;

(5) Find and determine the optimal parameters C and g;

(6) Select the optimal solution C and g, and establish the PSO-KELM regression model.

After we obtain the PSO-KELM model, we need to calculate the evaluation index of the model and analyze the results. Finally, we get the optimal error compensation method we need.

3) EVALUATION INDEX

The effect of wind speed error compensation is determined by the comparison of the evaluation indexes, such as mean absolute percentage error (MAPE), mean absolute error (MAE) and R-Square (R^2).

The formula of MAPE is as follow:

$$MAPE = \frac{100\%}{z} \sum_{p=1}^{z} \left| \frac{\hat{q}_p - q_p}{q_p} \right| \tag{9}$$

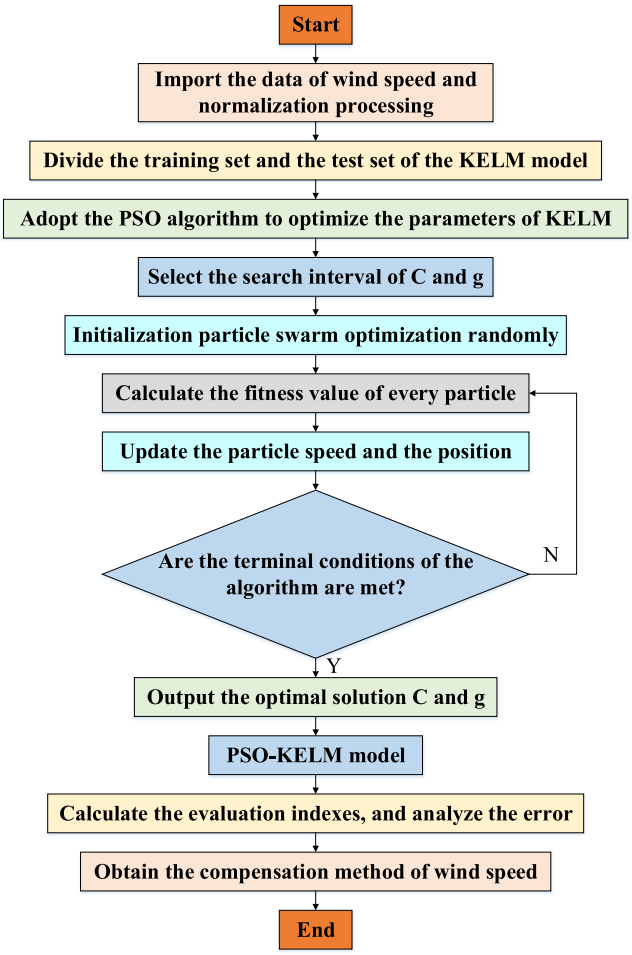

FIGURE 4. The processing flow of the PSO-KELM regression model.

The formula of MAE is as follow:

$$MAE = \frac{1}{z} \sum_{p=1}^{z} |\hat{q}_p - q_p| \tag{10}$$

The formula of R^2 is as follow:

$$R^2 = \frac{\sum_{p=1}^{z} (\hat{q}_p - \bar{q}_p)^2}{\sum_{p=1}^{z} (\bar{q}_p - q_p)^2} \tag{11}$$

where z is number of samples, $\hat{q}_p$ is the processed value, q_p is the actual value, $\bar{q}_p$ is the average value of the actual value.

In the process of evaluation, the better the smaller the value of the MAPE and MAE, and the R^2 just the opposite.

III. MODELING AND SIMULATION

A. HARDWARE AND APPEARANCE DESIGN

1) HARDWARE DESIGN

Figure 5 shows the schematic block diagram of the ultrasonic anemometer. When we design and develop the ultrasonic anemometer, we choose the STM32F103 microprocessor as

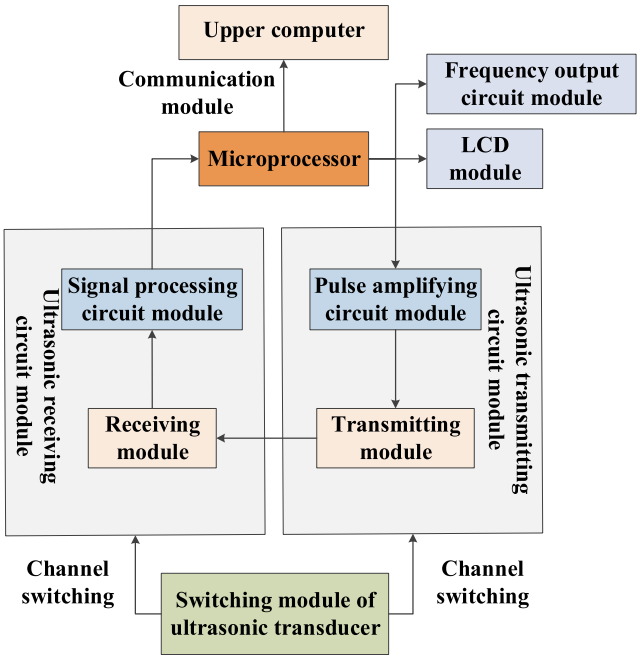

FIGURE 5. Schematic block diagram of ultrasonic anemometer.

the control core. And it is equipped with many functional modules, such as Ultrasonic transmitting and receiving, Frequency output, LCD, Communication, etc. Keil μ Vision5 is selected as an integrated development environment. Meanwhile, we also set up the upper computer system. To ensure the safety of workers, we deal with the intrinsic safety of the ultrasonic anemometer.

2) APPEARANCE DESIGN

The wind direction of the coal mine roadway is single. Considering the practicability and portability of the equipment, we design the appearance of the ultrasonic anemometer reliably. Figure 6 is the physical diagram and three views of the ultrasonic anemometer designed by our team. It consists of an upper shell, a lower shell, and a battery back cover. The radius of the ultrasonic sensor is 3mm, the inner diameter of the upper cylinder is 40mm, and the outer diameter is 54.5mm. The height of the whole ultrasonic anemometer is 200mm, and the distance between each pair of opposite-type ultrasonic probes is 84.62mm.

B. MODELING AND SIMULATION

1) MODELING AND MESHING

While building the hardware model, we need to build the simulation model with Fluent software. The purpose of building the simulation model is to obtain the wind speed data and provide the sample data for the algorithm model. Then we can obtain the error compensation method accurately. The flow chart of the simulation established by CFD software is shown in Figure 7.

Based on the requirements of the ultrasonic anemometer's hardware model, we design it by SOLIDWORKS.

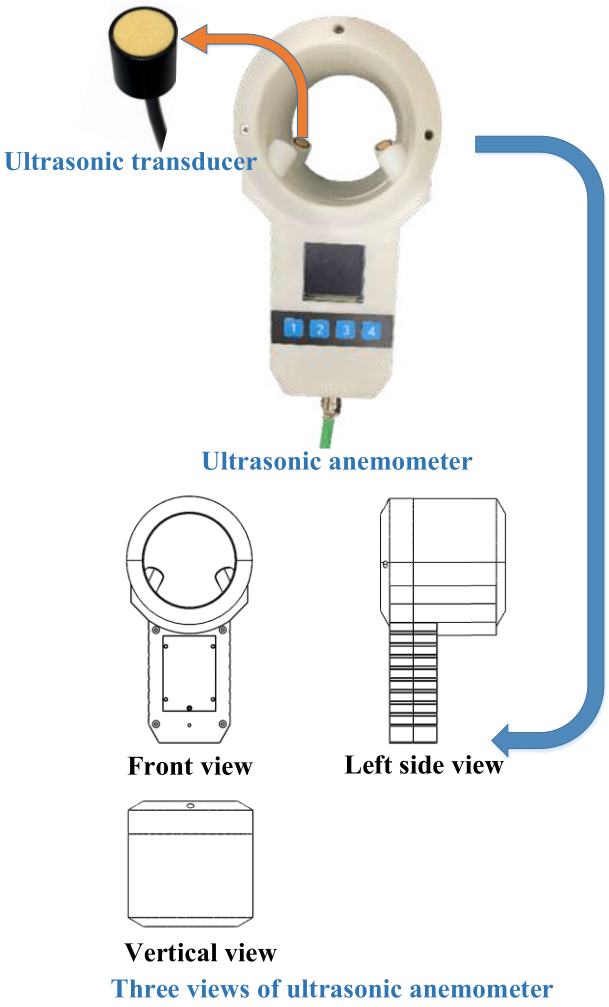

FIGURE 6. Physical drawing and three views of the ultrasonic anemometer.

We import the file exported from SOLIDWORKS into Gambit software and carry out the simulation of experiments in the wind tunnel. Figure 8 shows the air domain model created in Gambit software. In the process of building the air domain, the larger air domain can improve the calculation accuracy, but also increase the amount of calculation. When the size of the air region is ten times that of the device model, the accuracy is enough for the calculation requirements. Based on this, the wind tunnel model is a cylinder with a height of 2m and a radius of 1m. After building the air domain model, we import it into Workbench 14.5 for boundary setting and mesh generation.

Before we carry out the calculation of the finite volume method, it is necessary to mesh the model before CFD simulation. Figure 9 shows the grid division of ultrasonic anemometer model. The upside of Figure 9 shows the grid division of the computational domain. The inlet is the air intake, and the outlet is the air outlet. We establish the wall named wall-wai in the wind tunnel at the same time. The

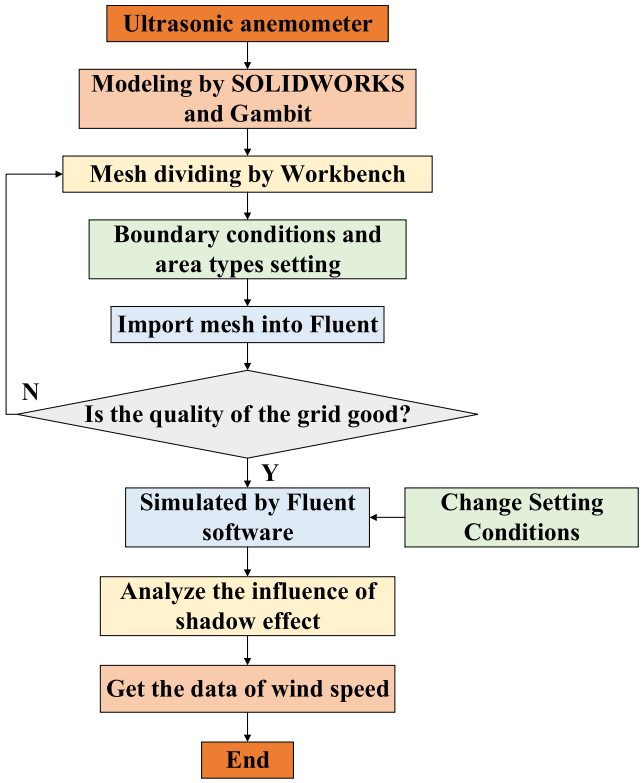

FIGURE 7. The flow chart of the simulation established by Fluent.

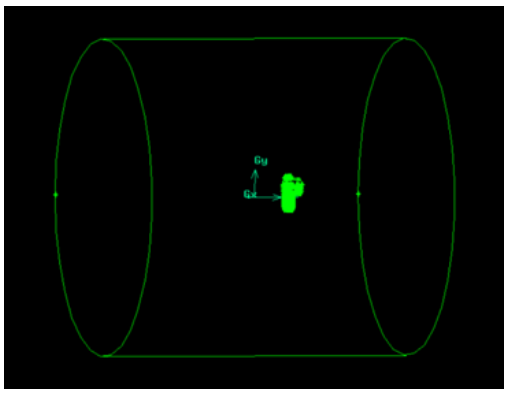

FIGURE 8. Air domain model created by Gambit.

calculation area is so large. To see the grid division clearly, the grid division around the ultrasonic anemometer shows in the lower part of Figure 9. The middle part on the upside of Figure 9 is the ultrasonic anemometer, and its periphery is the air domain. The model adopts a non-uniform grid division. Not only can we simulate the changes of the flow field near the ultrasonic anemometer accurately, but also we can reduce the calculation time of the simulation.

2) SIMULATION AND RESULT ANALYSIS

In the paper, the wind field distribution of the ultrasonic anemometer and its vicinity were simulated by Fluent software. When the wind speed is low, the trajectory of fluid particles is a regular smooth curve, which is called laminar.

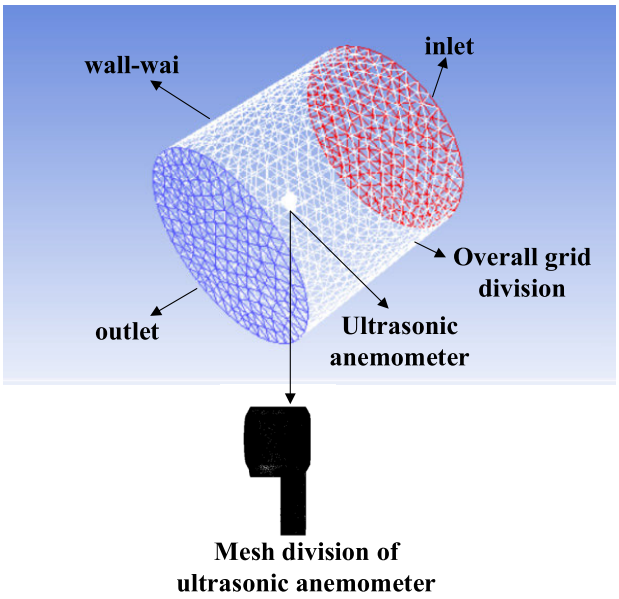

FIGURE 9. Grid division of ultrasonic anemometer model.

When the wind speed exceeds a certain range, the trajectory of fluid particles presents an irregular flow, and vortices appear in the flow field. This phenomenon is called turbulence. In hydrodynamics, Reynolds number (Re) is used to divide laminar and turbulence, and the formula is as follow:

$$\mathrm{Re} = \frac{\rho v D}{\mu} \tag{12}$$

where ρ is the fluid density, v is the fluid velocity, D is the characteristic length, μ is the viscosity coefficient of the fluid. When the Reynolds number is small, the laminar model is used for the simulation. As the wind speed increases, so does the Reynolds number. When the flow state of the fluid is converted to turbulence, we need to add the governing equation of turbulence. After the grid file was imported into Fluent, we can calculate the Reynolds number according to the solid calculation model of the ultrasonic anemometer. When the wind speed is less than 0.17m/s, we use the laminar model for simulation. And when the measured wind speed value is more than 0.17m/s, we use the k-ε model for simulation. The air inlet and outlet are set to velocity type and pressure type respectively. Because of the large number of grids, the number of iterations sets to 400.

Figure 10 shows the velocity cloud of the Fluent simulation. At this time, the input wind speed is 10 m/s. On the left side of the graph, the color distribution changes with the speed value. The dark part is the area affected by the shadow effect. According to the theoretical method proposed above, we can calculate the wind speed affected by the shadow effect.

IV. RESULTS AND DISCUSSION

A. ACQUISITION OF EXPERIMENTAL DATA

By dividing the wind measurement path equally and substituting wind speed data of each point obtained from Fluent

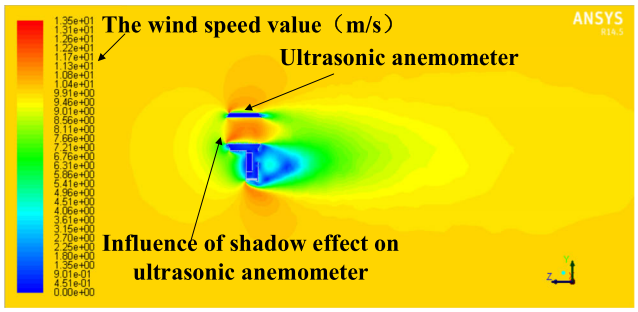

(a) Side view of wind field distribution around ultrasonic anemometer and its vicinity

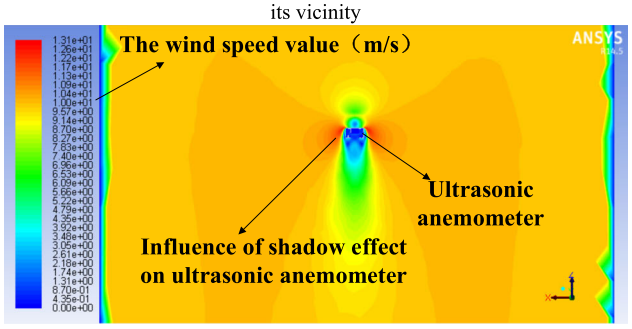

(b) Top view of wind field distribution around ultrasonic anemometer and its vicinity

FIGURE 10. Wind field distribution of ultrasonic anemometer and its vicinity.

TABLE 2. Conditions and parameters of the test in the wind tunnel.

Experimental conditions	Parameter	Experimental conditions	Parameter
Wind tunnel model	DHS-500*500/700*700-II	Coefficient of Pitot tube	1
Equipment model	AFP-6	Velocity ratio	1.97
	2239	Atmospheric pressure(hPa)	1020.79
Accuracy	Grade1	Temperature（℃）	19.1
	0.1 级	Humidity（%RH）	43.5

software into formulas, we can calculate the accurate wind speed data through the ultrasonic time-difference formula. Each experiment in the paper has run several times independently. All the experiments in this work are carried out on a personal computer with AMD Ryzen 54600h with a radon graphics processor, 3 GHz, 16GB RAM, and we take Windows 10 as the operating system. In addition, we carried out the wind tunnel test in Huaibei Engineering Testing Co., Ltd., which is located in Anhui Province, China. And we use the mine ultrasonic anemometer developed by our team. The conditions and parameters of the test in the wind tunnel are shown in Table 2.

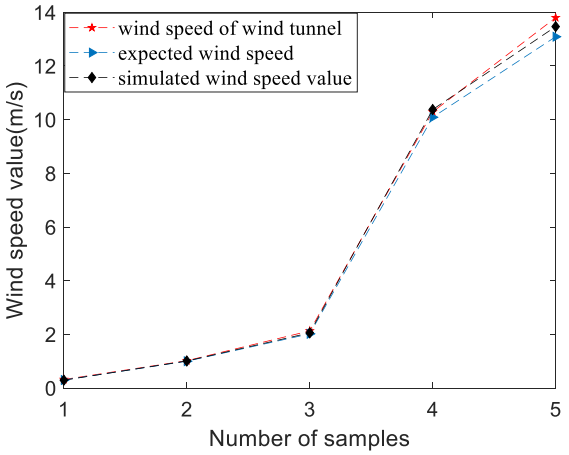

FIGURE 11. Comparison of simulated wind speed, wind speed of wind tunnel, and expected wind speed.

Due to the complexity of the test in the wind tunnel, when we change the input wind speed, it will take a long time for us to make the wind tunnel stable. Therefore, we select 0.3m/s, 1.0m/s, 2.02m/s, 10.09m/s and 13.09m/s as the wind tunnel input wind speed. At this time, the display values of the ultrasonic anemometer are 0.32m/s, 1.02m/s, 2.13m/s, 10.29m/s and 13.80m/s, respectively. All the input wind speed cited above have been simulated by Fluent software at the same time, and we compare the calculated wind speed data with the data of the wind tunnel measured in the field. The result is shown in Figure 11.

In Figure 11, the wind speed of the wind tunnel is the wind speed value measured by the ultrasonic anemometer in the wind tunnel, simulated wind speed is the wind speed value calculated by the Fluent software, and expected wind speed is wind speed which we want to get. Due to the interference of shadow effect on wind speed measurement, there is a deviation between expected wind speed and wind speed of wind tunnel. But the simulated wind speed value is in good agreement with the wind speed of the wind tunnel. It shows that the sample data used to build the PSO-KELM model in the paper are accurate and reliable.

Figure 12 shows the comparison between actual wind speed and expected wind speed. The actual wind speed is the value of the wind speed simulated by Fluent, and the expected wind speed is the real value that we want to get. When the expected wind speed is 5m/s and 15m/s, the actual wind speed is 5.1294m/s and 15.4366m/s separately. In the following, we will use the data of wind speed simulated by Fluent as the input data, and we take the expected wind speed as the fitting target. Based on this, we can complete the goal of error compensation for wind speed.

B. THE RESEARCH BASED ON KELM FOR ERROR COMPENSATION OF WIND SPEED

In the paper, the samples of the wind speed obtained by Fluent were divided into 140 training samples and 60 test

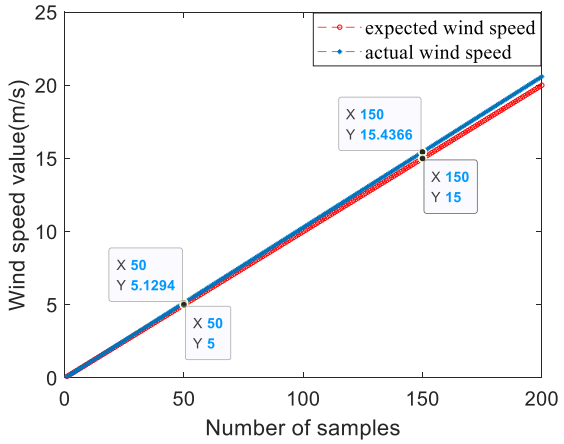

FIGURE 12. Actual wind speed and expected wind speed.

samples. And each regression model tests 50 times. We get the corresponding average values of MAPE, MAE, and R^2, and compare the performance of KELM, SVR, ELM, and BP, DT regression models. The comparison of MAE, MAPE, and R^2 of KELM, BP, SVR, ELM, and DT regression models shows in Table 3. Each regression model trains 50 times independently, and We choose the model with the lowest MAPE value for analysis. The number of hidden layer nodes of ELM is 3, while that of BP is 9.

TABLE 3. Comparison of prediction results of five regression models.

Model	Time/s	Train			Test		
		R^2	MAE	MAPE	R^2	MAE	MAPE
BP	0.1359	0.9932	0.3203	23.3074%	0.9933	0.3015	7.3260%
KELM	0.0008	0.9928	0.3177	12.0567%	0.9983	0.1750	2.9038%
SVR	0.0095	0.9944	0.3820	19.9946%	0.9943	0.3453	8.8344%
ELM	0.0004	0.9972	0.1811	10.3727%	0.9814	0.6105	13.8386%
DT	0.0055	0.9978	0.2248	6.0345%	0.9949	0.3301	6.8512%

On the test set, the average MAPE of KELM was 2.9038%. When SVR, BP, DT, and ELM regression models were used to predict the wind speed, the MAPE of the test set was 8.8344%, 7.3260%, 6.8512%, and 13.8386%, respectively, which was much higher than KELM's. In addition, the MAE is similar to the MAPE. The MAE of the KELM is 0.1750. The value of MAE of the KELM is much smaller than other regression algorithms. The opposite is true for R^2, and the R^2 of the KELM is the largest among several algorithms. By comparing the MAPE, MAE, and R^2 of the regression models, we can find that KELM has the best effect on error compensation of wind speed in the test set.

Comparing the prediction time of each regression model, we can see that the prediction time of the BP regression model is 0.1359s. It is the longest, and it is much longer than that of other regression models. The prediction time of ELM is 0.0004s, and it is the shortest. But the MAPE of ELM is much higher than other regression models, and the prediction effect of the ELM is poor. Since the ELM selects weights in the hidden layer randomly, it leads to the poor generalization ability of the algorithm. The KELM not only has the lowest MAPE value, but also its prediction time is only 0.0008s.

Based on the above analysis, the Figure 13 shows the comparison among the corrected wind speed, actual wind speed, and expected wind speed of five regression models on the test set. In Figure 13, actual wind speed is the wind speed value calculated by the Fluent software, corrected wind speed is the wind speed value corrected by the regression model, and expected wind speed is wind speed which we want to get. We can see that the effect of error compensation for the wind speed of SVR, DT, and ELM is poor. In the SVR model, when the wind speed is high, the corrected wind speed of the sample point is lower than the expected wind speed, while when the wind speed is low, the corrected wind speed of the sample point is higher than the expected wind speed. As we can see, the corrected wind speed and expected wind speed of the SVR fit well in the range of 7 to 12 m/s. In Figure 13, compared with other regression models, the corrected wind speed of the KELM model has the best fitting degree with the expected wind speed in the whole range of the wind speed. The KELM uses the method of stable kernel mapping, and it has the advantages of fast convergence. And the data in the paper is simple. Based on these, the KELM model can get good results.

C. ERROR COMPENSATION FOR THE WIND SPEED OF KELM WITH PARAMETER OPTIMIZATION

The purpose of the paper is to compensate for the error of the wind speed of the ultrasonic anemometer so that we can make the measurement result more accurate. When we use the KELM regression model to compensate for the error of the wind speed, the average value of MAPE is 2.9038%. It is still large, so we need to optimize the parameters of KELM further. The PSO optimization algorithm performs well in practical applications. Based on this, the paper uses the PSO optimization algorithm to find the best parameters of the model.

1) ERROR COMPENSATION IN WIND SPEED BASED ON PSO-KELM

When the parameters of KELM optimize by PSO, the maximum number of iterations is 100, and the initial number of particles is 10. The initial value of C and g are 1 and 100, respectively. The optimization range of parameter C is $[2^{-8}, 2^8]$, and the optimization range of parameter g is $[2^{-6}, 2^6]$. The optimization curve of the KELM model optimized by PSO shows in Figure 14. We can see that the PSO algorithm performs well in KELM's optimization, and the model can converge to the optimal value quickly. At the beginning of the iteration of the PSO algorithm, the R^2 of the test set reaches more than 0.99. And it converges to the global optimum when the number of iterations is 4. At this time, the R^2 is 0.9999,

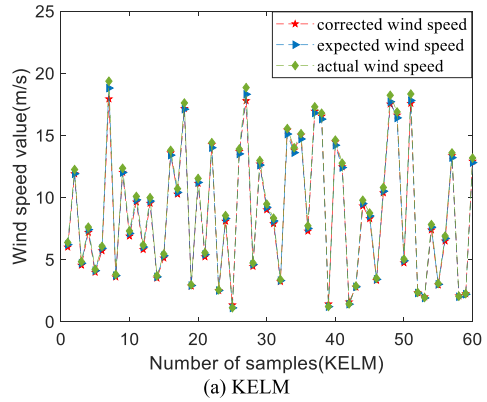

(a) KELM

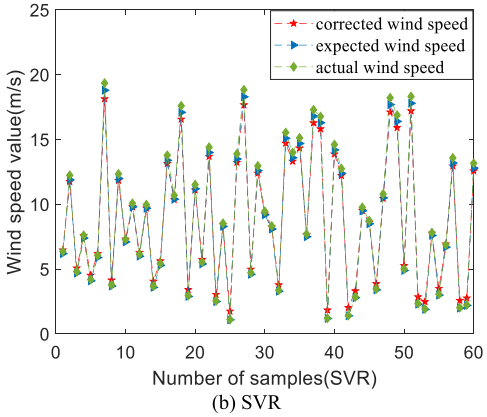

(b) SVR

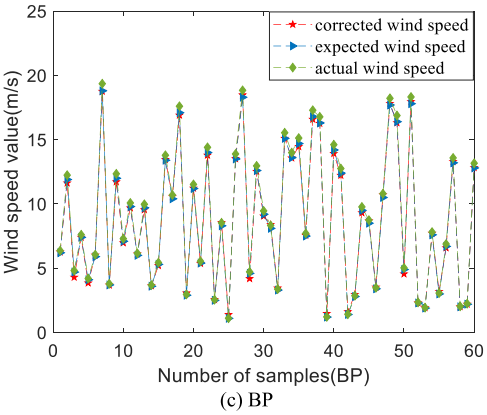

(c) BP

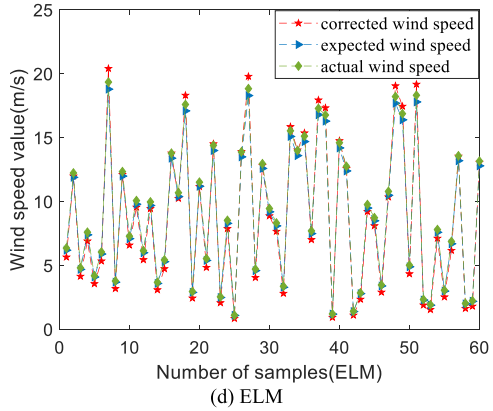

(d) ELM

FIGURE 13. Comparison of corrected wind speed, expected wind speed and actual wind speed of five regression model on the test sets. (a) KELM. (b) SVR. (c) BP. (d) ELM. (e) DT.

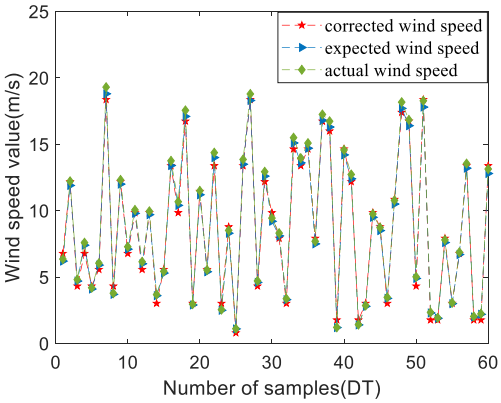

(e) DT

FIGURE 13. *(Continued.)* Comparison of corrected wind speed, expected wind speed and actual wind speed of five regression model on the test sets. (A) KELM. (B) SVR. (C) BP. (D) ELM. (E) DT.

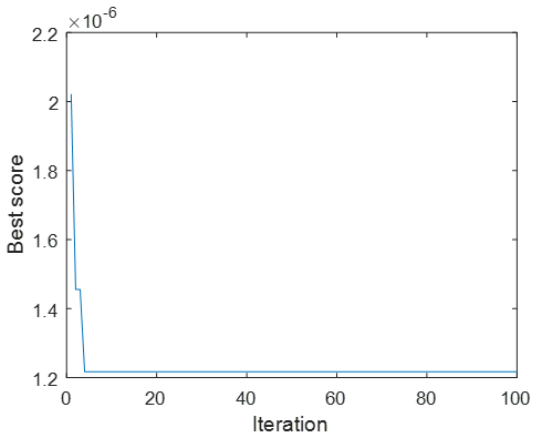

FIGURE 14. Optimization curve of KELM regression model optimized by PSO.

the optimal value of C is 91.9888, the optimal value of g is 1.3977, and the prediction time is 0.0058s.

The comparison of MAE, MAPE, and R^2 between PSO-KELM and KELM regression models shows in Table 4. In Table 4, PSO-KELM indicates that the parameters C and g of the KELM model are the optimal value. KELM indicates that the parameters C and g of the KELM model are default setting values. On the test set, the average MAPE of KELM is 2.9038%. After the parameters of KELM are optimized by the PSO algorithm, the average MAPE of PSO-KELM is 0.0974%. In other words, after parameter optimization, the prediction accuracy of KELM is greatly improved. Due to the PSO has the characteristics of fast convergence and strong global searchability. Based on the data in the paper, the PSO combined with the KELM model can achieve good results.

Figure 15 shows the comparison among the corrected wind speed, actual wind speed, and expected wind speed of the PSO-KELM regression model on the test set. In Figure 15, actual wind speed is the wind speed value calculated by the

TABLE 4. Comparison of prediction results of PSO-KELM and KELM.

Model	Time/s	Train			Test		
		R^2	MAE	MAPE	R^2	MAE	MAPE
KELM	0.00077	0.9928	0.3177	12.0567%	0.9983	0.1750	2.9038%
PSO-KELM	0.00083	1.0000	0.0146	0.3000%	1.0000	0.0083	0.0974%

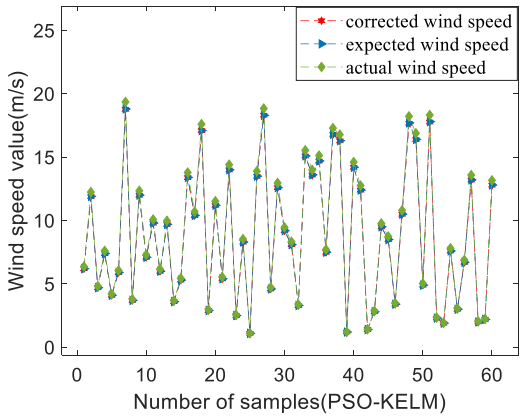

FIGURE 15. Comparison of corrected wind speed, expected wind speed, and actual wind speed of PSO-KELM regression model on the test set.

Fluent software, corrected wind speed is the wind speed value corrected by the PSO-KELM, and expected wind speed is wind speed which we want to get. We can see that the coincidence degree of the corrected wind speed and the expected wind speed of the sample points is very high, which indicates that the PSO-KELM regression model has a good effect on the error compensation of wind speed.

Figure 16 shows the relative error between the corrected wind speed and the expected wind speed of each regression model on the test set. After the correction of PSO-KELM, the relative error between the corrected wind speed and the expected wind speed is stable between −0.2% and 0.25%, and the relative error of the 25th sample data is the largest, which is 0.236%. At this time, the expected wind speed is 1.1m/s, the actual wind speed is 1.1111m/s, and the corrected wind speed is 1.1026m/s. The relative error of the 18th sample data is the smallest, and the value is −0.023%. At this time, the expected wind speed is 17.1m/s, the actual wind speed is 17.6008m/s, and the corrected wind speed is 17.0961m/s. As we can see, the corrected wind speed is very close to the expected wind speed. Compared with the PSO-KELM regression model, the relative error between the wind speed corrected by other regression models and the expected wind speed is larger. Among them, the relative error of the 25th sample data in KELM, SVR, and BP models is the largest, reaching 21.8581%, 59.2806%, and 26.4634%, respectively. At this time, the expected wind speed is small, which is 1.1m/s. The relative error of the 59th sample data in the ELM model is the largest, which is −28.3678%. The relative error of the 39th sample data in the DT model is the largest, which is 47.6190%. In Figure 16, we can more intuitively see that the error compensation effect of PSO-KELM is the best in the paper.

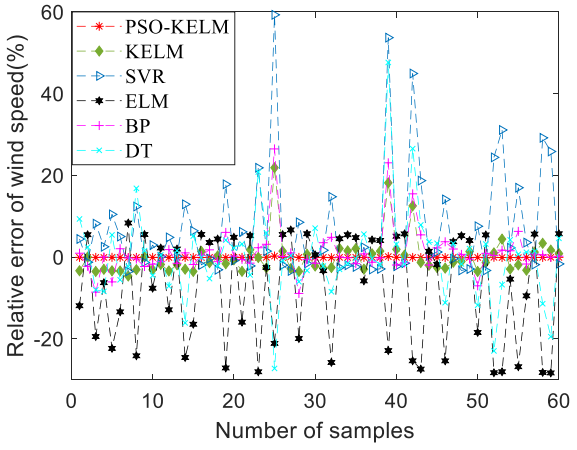

FIGURE 16. The relative error between the corrected wind speed and the expected wind speed of each regression model on the test set.

2) STATISTICAL TEST

In order to ensure the superiority of the PSO-KELM model, we also carried out some calculations in a statistical test. We adopt the method of the independent sample t-test in statistical tests to process the results of the above regression models. The comparison of multiple regression models in the independent sample t-test is shown in Table 5. In Table 5, the P-value indicates that the probability of sample observations or more extreme results when the original hypothesis is true. If the P-value is very small, it means that the probability of the original hypothetical situation is very small. The smaller the p-value, the more sufficient the reason for rejecting the original hypothesis. The P-value of the PSO-KELM is 0.993, which is greater than 0.05. This shows that there is no significant difference between the output data of the PSO-KELM model and the expected data under the 99.3% confidence interval.

TABLE 5. Comparison of multiple regression models in independent sample t-test.

Category	Results		
	average value	standard deviation	P-value
Expected value	8.808333333	5.256933812	\
PSO-KELM	8.800490264	5.252102241	0.993
KELM	8.75406276	5.266389712	0.955
SVR	8.888299849	4.867604275	0.931
BP	8.836841142	5.146114317	0.976
ELM	8.871360971	5.603970809	0.949
DT	8.802806878	5.265205021	0.995

As we can see, the P values of all regression models used in the paper were greater than 0.05. The average value and standard deviation of the PSO-KELM are close to that of the Expected value. The P-value of the DT model is the largest. However, the smaller P does not mean that the actual difference is greater, but the more reason to explain that there is a difference between the two. Whether the difference is statistically significant or not and whether there is professional actual significance are not exactly the same. Although the P-value of the PSO-KELM model is less than that of the DT model, the MAPE, MAE, and other evaluation indexes of the PSO-KELM model are less than that of the DT model. In a word, the compensation effect of the PSO-KELM model is better than other regression models in the paper.

3) THE ACCURACY VERIFICATION OF THE PSO-KELM REGRESSION MODEL

In the previous paper, based on the data simulated from Fluent, we verified the superiority of the error compensation effect of the PSO-KELM regression model. In this section, we check the accuracy of the PSO-KELM regression model by combining the data measured by the ultrasonic anemometer in the wind tunnel further. In Figure 17, the left axis is the wind speed value, and it shows the comparison between the corrected wind speed, expected wind speed, and actual wind speed of the PSO-KELM on the test set. In Figure 17, actual wind speed is the wind speed value measured by the ultrasonic anemometer in the wind tunnel, corrected wind speed is the wind speed value corrected by the PSO-KELM, and expected wind speed is wind speed which we want to get. The right axis is the relative error of wind speed. And it shows the relative error between the actual wind speed and the expected wind speed, and the relative error between the wind speed corrected by the PSO-KELM and the expected wind speed, and the difference between the two relative errors. We can see that the corrected wind speed tends to the expected wind speed after the actual wind speed obtained in the wind tunnel input into the PSO-KELM regression model. The relative error of the first sample data is the largest, which is 9.3549%. At this time, the expected wind speed is 0.3m/s, and the absolute error between the corrected wind speed and the expected wind speed is 0.02806m/s. The reason for the larger relative error is that the expected wind speed is small. The relative error between the corrected wind speed and the expected wind speed is between -0.4% and 10%. And the coincidence degree of the corrected wind speed and the expected wind speed of the sample points is very high. In Figure 17, we can see that the PSO-KELM regression model is also effective for the error compensation of data obtained by the ultrasonic anemometer in the wind tunnel. The PSO-KELM regression model can improve the measurement accuracy of the ultrasonic anemometer. The research results of the paper have the reference value for the development of the high-precision ultrasonic anemometer.

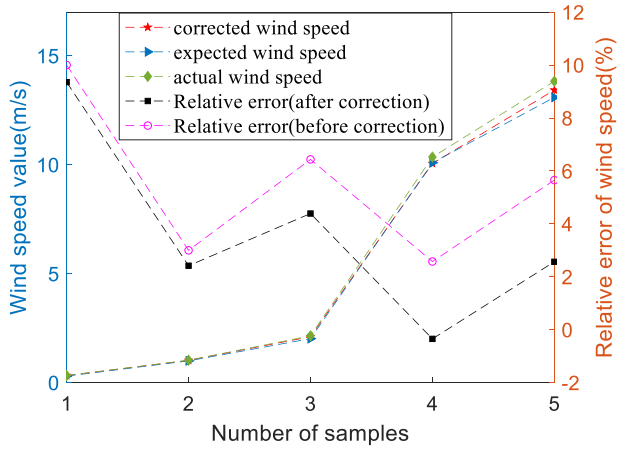

FIGURE 17. Accuracy verification of PSO-KEIM regression model based on the data obtained in the wind tunnel.

V. CONCLUSION

To compensate for the error of wind speed caused by the shadow effect, we propose a method based on kernel extreme learning machine combined with particle swarm optimization. Firstly, it is difficult to obtain the wind speed data in the field, and the time cost is very high. Therefore, we use CFD to simulate the measurement scene of the ultrasonic anemometer in the wind tunnel and analyze the influence of the shadow effect. Then, the KELM regression model is established based on the data simulated by Fluent. In order to achieve the best result of error compensation for wind speed, we also use SVR, BP, DT, and ELM to compensate for the wind speed data. The MAPE of the KELM is 2.9038%, and it is smaller than that of other models. In order to improve the error compensation effect of the KELM regression model for the wind speed further, we use the PSO algorithm to search KELM's parameters automatically and then build the PSO-KELM regression model. Finally, based on the theoretical analysis and simulation verification, we further verify the accuracy of the PSO-KELM regression model by combining the measured data obtained in the wind tunnel.

The results show that (1) It is effective to use the simulation data to study the influence of shadow effect of ultrasonic anemometer; (2) The PSO algorithm can effectively optimize the parameters of the model, and improve the efficiency and reliability of modeling; (3) The KELM model has high prediction accuracy and short training time, which effectively avoids overfitting and has a certain generalization ability; (4) The PSO-KELM regression model can effectively improve the accuracy of the ultrasonic anemometer, and it makes the measurement results of the ultrasonic anemometer more accurate. The PSO-KELM regression model proposed in the paper can effectively compensate for the error of wind speed. The research of the paper has a significant value for the workers to measure the wind speed in the coal mine roadway accurately.

REFERENCES

[1] J. Cheng and S. Yang, "Data mining applications in evaluating mine ventilation system," *Saf. Sci.*, vol. 50, no. 4, pp. 918–922, Apr. 2012.

[2] N. Wenyao, L. Baokuan, and G. Wenmei, "The research on integrated visual information management system of the mine ventilation and safety," *Procedia Eng.*, vol. 26, pp. 2070–2074, 2011.

[3] R. Huang, X. Shen, B. Wang, and X. Liao, "Migration characteristics of CO under forced ventilation after excavation roadway blasting: A case study in a plateau mine," *J. Cleaner Prod.*, vol. 267, Sep. 2020, Art. no. 122094.

[4] L. Yiding, W. Baoqiang, and W. Yanjie, "Time-difference ultrasonic wind detection methods based on cross-correlation theory," in *Proc. 8th Int. Conf. Electron. Meas. Instrum.*, Aug. 2007, pp. 1-165–1-168.

[5] D. Fernandes, L. Gomes, and A. Costa, "Wind speed and direction measurement based on time of flight ultrasonic anemometer," in *Proc. IEEE 26th Int. Symp. Ind. Electron. (ISIE)*, Jun. 2017, pp. 1417–1422.

[6] X. Li, G. Zhu, W. Gao, H. Sun, G. Liu, Y. Wu, and Y. Shi, "A novel ultrasonic array signal processing scheme for wind measurement," *ISA Trans.*, vol. 81, pp. 259–269, Oct. 2018.

[7] D. Xi-Bo, Z. Yi-Feng, L. Chun-Yu, and W. Jian, "Study of the ultrasonic three-dimensional wind speed measurement methods based on the phase difference," in *Proc. 6th Int. Conf. Instrum. Meas., Comput., Commun. Control (IMCCC)*, Jul. 2016, pp. 785–789.

[8] G. M. G. Lopes, D. P. da Silva, J. A. de França, M. B. de Morais França, L. de Souza Ribeiro, M. Moreira, and P. Elias, "Development of 3-D ultrasonic anemometer with nonorthogonal geometry for the determination of high-intensity winds," *IEEE Trans. Instrum. Meas.*, vol. 66, no. 11, pp. 2836–2844, Nov. 2017.

[9] T. W. Horst, S. R. Semmer, and G. Maclean, "Correction of a non-orthogonal, three-component sonic anemometer for flow distortion by transducer shadowing," *Boundary-Layer Meteorol.*, vol. 155, no. 3, pp. 371–395, Feb. 2015.

[10] M. Ghaemi-Nasab, S. Franchini, F. Sorribes-Palmer, and A. R. Davari, "A calibration procedure to correct the shadow effect in ultrasonic wind sensors," *J. Wind Eng. Ind. Aerodyn.*, vol. 179, pp. 475–482, Aug. 2018.

[11] Y. Yang and X. Chen, "Shadow effect compensation method for ultrasonic transducer array model," *Vibroeng. Procedia*, vol. 28, pp. 148–153, Oct. 2019.

[12] F. Hu, M. Zhou, P. Yan, K. Bian, and R. Dai, "Multispectral imaging: A new solution for identification of coal and gangue," *IEEE Access*, vol. 7, pp. 169697–169704, Nov. 2019.

[13] F. Hu, M. Zhou, P. Yan, K. Bian, and R. Dai, "PCANet: A common solution for laser-induced fluorescence spectral classification," *IEEE Access*, vol. 7, pp. 107129–107141, 2019.

[14] K. Bian, M. Zhou, F. Hu, and W. Lai, "RF-PCA: A new solution for rapid identification of breast cancer categorical data based on attribute selection and feature extraction," *Frontiers Genet.*, vol. 11, Sep. 2020, Art. no. 566057.

[15] K. Bian, M. Zhou, F. Hu, W. Lai, and M. Huang, "CEEMD: A new method to identify mine water inrush based on the signal processing and laser-induced fluorescence," *IEEE Access*, vol. 8, pp. 107076–107086, Jun. 2020.

[16] M. S. Ahmad, S. M. Adnan, S. Zaidi, and P. Bhargava, "A novel support vector regression (SVR) model for the prediction of splice strength of the unconfined beam specimens," *Construct. Building Mater.*, vol. 248, Jul. 2020, Art. no. 118475.

[17] X. Zheng, W. Lai, H. Chen, and S. Fang, "Data prediction of mobile network traffic in public scenes by SOS-vSVR method," *Sensors*, vol. 20, no. 3, p. 603, Jan. 2020.

[18] S. R. Das, D. Mishra, and M. Rout, "A hybridized ELM-jaya forecasting model for currency exchange prediction," *J. King Saud Univ.-Comput. Inf. Sci.*, vol. 32, no. 3, pp. 345–366, Mar. 2020.

[19] H. Du, D. Song, Z. Chen, H. Shu, and Z. Guo, "Prediction model oriented for landslide displacement with step-like curve by applying ensemble empirical mode decomposition and the PSO-ELM method," *J. Cleaner Prod.*, vol. 270, Oct. 2020, Art. no. 122248.

[20] S. Yu, K. Zhu, and F. Diao, "A dynamic all parameters adaptive BP neural networks model and its application on oil reservoir prediction," *Appl. Math. Comput.*, vol. 195, no. 1, pp. 66–75, Jan. 2008.

[21] J. Yi, Q. Wang, D. Zhao, and J. T. Wen, "BP neural network prediction-based variable-period sampling approach for networked control systems," *Appl. Math. Comput.*, vol. 185, no. 2, pp. 976–988, Feb. 2007.

[22] M. Hammed and S. Jumoke, "An implementation of decision tree algorithm augmented with regression analysis for fraud detection in credit card," *Int. J. Comput. Sci. Inf. Secur.*, vol. 18, no. 2, pp. 79–88, Feb. 2020.

[23] H. Che, S. Ou, and H. Wei, "Predicting fish ecological as indicator of river pollution using decision tree technique," in *Proc. IOP Conf.: Earth Environ. Sci.*, vol. 164, 2018, Art. no. 012022.

[24] F. Karimi, S. Sultana, A. Babakan, and S. Shan, "Urban expansion modeling using an enhanced decision tree algorithm," *GeoInformatica*, vol. 2019, pp. 1–17, Aug. 2019.

[25] K. Li, W. Xu, Y. Han, F. Ge, and Y. Wang, "A hybrid modeling method for interval time prediction of the intermittent pumping well based on IBSO-KELM," *Measurement*, vol. 151, Feb. 2020, Art. no. 107214.

[26] K. Ding, X. Chen, J. Zhang, L. Feng, F. U. Hamelmann, and S. Weng, "Photovoltaic array power prediction model based on EEMD and PSO-KELM," in *Proc. 47th IEEE Photovoltaic Spec. Conf. (PVSC)*, Jun. 2020, pp. 2532–2537.

[27] X. Zheng, W. Lai, H. Chen, S. Fang, and Z. Li, "A study of cellular traffic data prediction by kernel ELM with parameter optimization," *Appl. Sci.*, vol. 10, no. 10, p. 3517, May 2020.

[28] S. Lu, H. Yu, H. Dong, X. Wang, and Y. Sun, "Single-step prediction method of burning zone temperature based on real-time wavelet filtering and KELM," *Eng. Appl. Artif. Intell.*, vol. 70, pp. 142–148, Apr. 2018.

[29] S. Shamshirband, K. Mohammadi, H.-L. Chen, G. N. Samy, D. Petkovi, and C. Ma, "Daily global solar radiation prediction from air temperatures using kernel extreme learning machine: A case study for Iran," *J. Atmos. Sol.-Terr. Phys.*, vol. 134, pp. 109–117, Nov. 2015.

[30] Q. Fu, W. Shen, X. Wei, Y. Zhang, H. Xin, Z. Su, and C. Zhao, "Prediction of the diet energy digestion using kernel extreme learning machine: A case study with Holstein dry cows," *Comput. Electron. Agricult.*, vol. 169, Feb. 2020, Art. no. 105231.

[31] R. Liu, Y. Wang, H. Zhou, and Z. Qian, "Short-term passenger flow prediction based on wavelet transform and kernel extreme learning machine," *IEEE Access*, vol. 7, pp. 158025–158034, Oct. 2019.

[32] W. Fu, K. Wang, J. Tan, and K. Zhang, "A composite framework coupling multiple feature selection, compound prediction models and novel hybrid swarm optimizer-based synchronization optimization strategy for multi-step ahead short-term wind speed forecasting," *Energy Convers. Manage.*, vol. 205, Feb. 2020, Art. no. 112461.

[33] Y. Chen, J. Fan, Z. Deng, B. Du, X. Huang, and Q. Gui, "PR-KELM: Icing level prediction for transmission lines in smart grid," *Future Gener. Comput. Syst.*, vol. 102, pp. 75–83, Jan. 2020.

[34] Y. Ding, W. Zhang, L. Yu, and K. Lu, "The accuracy and efficiency of GA and PSO optimization schemes on estimating reaction kinetic parameters of biomass pyrolysis," *Energy*, vol. 176, pp. 582–588, Jun. 2019.

[35] G. Yuan and W. Yang, "Study on optimization of economic dispatching of electric power system based on hybrid intelligent algorithms (PSO and AFSA)," *Energy*, vol. 183, pp. 926–935, Sep. 2019.

[36] W. Zhu, H. Nikafshan Rad, and M. Hasanipanah, "A chaos recurrent ANFIS optimized by PSO to predict ground vibration generated in rock blasting," *Appl. Soft Comput.*, vol. 108, Sep. 2021, Art. no. 107434.

[37] X. Tang, Q. Guo, M. Li, C. Wei, Z. Pan, and Y. Wang, "Performance analysis on liquid-cooled battery thermal management for electric vehicles based on machine learning," *J. Power Sources*, vol. 494, May 2021, Art. no. 229727.

[38] K. Synylo, A. Krupko, O. Zaporozhets, and R. Makarenko, "CFD simulation of exhaust gases jet from aircraft engine," *Energy*, vol. 213, Dec. 2020, Art. no. 118610.

[39] C. Gromke, B. Blocken, W. Janssen, B. Merema, T. V. Hooff, and H. Timmermans, "CFD analysis of transpirational cooling by vegetation: Case study for specific meteorological conditions during a heat wave in Arnhem, Netherlands," *Building and Environ.*, vol. 83, pp. 11–26, Jan. 2015.

[40] K.-H. Kwak, J.-J. Baik, Y.-H. Ryu, and S.-H. Lee, "Urban air quality simulation in a high-rise building area using a CFD model coupled with mesoscale meteorological and chemistry-transport models," *Atmos. Environ.*, vol. 100, pp. 167–177, Jan. 2015.

[41] S. Echi, A. Bouabidi, Z. Driss, and M. S. Abid, "CFD simulation and optimization of industrial boiler," *Energy*, vol. 169, pp. 105–114, Feb. 2019.

[42] S. Liu, W. Pan, X. Zhao, H. Zhang, X. Cheng, Z. Long, and Q. Chen, "Influence of surrounding buildings on wind flow around a building predicted by CFD simulations," *Building Environ.*, vol. 140, pp. 1–10, Aug. 2018.

[43] S. Dixit, A. Kumar, S. Kumar, N. Waghmare, H. C. Thakur, and S. Khan, "CFD analysis of biodiesel blends and combustion using ansys fluent," *Mater. Today: Proc.*, vol. 26, pp. 665–670, 2020.

ZHENGUAN CAO received the Ph.D. degree from China University of Mining and Technology. He is currently an Associate Professor with Anhui University of Science and Technology. His research interests include image processing, machine learning, and coal mine safety monitoring and control.

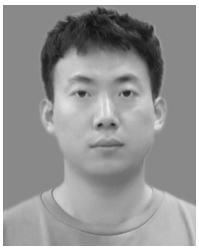

ZONGTANG ZHANG is currently pursuing the master's degree with Anhui University of Science and Technology. His research interests include machine learning, intelligent control, and circuits and systems.

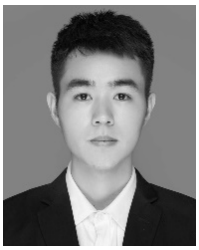

RUI LI is currently pursuing the master's degree with Anhui University of Science and Technology. His research interests include intelligent control, image processing, and integrated circuit technology.

XUN YANG is currently pursuing the master's degree with Anhui University of Science and Technology. His research interests include intelligent control, digital integrated circuits, and image analysis.

ZHENGHANG ZHOU is currently pursuing the master's degree with Anhui University of Science and Technology. His research interests include algorithms, artificial intelligence, and intelligent control.